

Interference Prediction in Wireless Networks: Stochastic Geometry meets Recursive Filtering

Jorge F. Schmidt, Udo Schilcher, Mahin K. Atiq, and Christian Bettstetter, *Senior Member, IEEE*

Abstract—This article proposes and evaluates a technique to predict the level of interference in wireless networks. We design a recursive predictor that computes future interference values at a given location by filtering measured interference at this location. The parametrization of the predictor is done offline by translating the autocorrelation of interference into an autoregressive moving average (ARMA) representation. This ARMA model is inserted into a steady-state Kalman filter enabling nodes to predict with low computational effort. Results show good performance in terms of accuracy between predicted and true values for relevant time horizons. Although the predictor is parametrized for the case of Poisson networks, Rayleigh fading, and fixed message lengths, a sensitivity analysis shows that it also works well in more general network scenarios. Numerical examples for underlay device-to-device communications and a common wireless sensor technology illustrate its broad applicability. The predictor can be applied as part of interference management to improve medium access, scheduling, and resource allocation.

Index Terms—Wireless systems, interference, prediction, stochastic geometry, ARMA, Kalman filter.

I. INTRODUCTION

A. Motivation and Related Work

The management of interference has always been an essential building block in the design and performance analysis of wireless communication systems. Its importance will even increase with the ongoing penetration of wireless connectivity into industrial domains subject to high reliability constraints.

There are various strategies to handle interference [1]: The choice of strategy mainly depends on the signal-to-interference ratio (SIR) at the receiver. If interference is very weak, it should be ignored and treated as noise. If interference is stronger—about as strong as the desired signal—we want to avoid it and allow only one node to transmit at a given time or frequency in a certain spatial region. A broad spectrum of such orthogonalization techniques has been developed and widely used for this purpose, including medium access control (MAC) protocols, scheduling, and radio resource allocation. If interference is even stronger than the signal of interest, it is favorable to allow interference and decode it at the receiver rather than to avoid it (see [2]–[4]). Besides solutions on minimizing the negative effects of interference, novel concepts have emerged that consider the positive rather than the negative aspects of interference and try to harness it for the benefit

of the network [1]. Examples include the use of interference for physical-layer security and energy harvesting from radio signals. From the viewpoint of energy harvesting, for instance, interference is a valuable source of energy that can be captured by devices. Another perspective on interference management is offered by interference alignment [5], which breaks with the capacity limits of conventional orthogonal multiple access techniques and is currently under intense investigation.

The paper at hand takes a very different perspective on managing interference: we propose and evaluate a technique for *interference prediction* that exploits analytical results on the modeling of interference using stochastic geometry.

In this context, interference is described as a random variable whose properties depend on several parameters including node locations, mobility, and data traffic patterns. These properties can be calculated in a given setup using tools from stochastic geometry. Examples include the mean interference (see [6], [7]), higher-order statistics [8], and distribution (see [9]–[13]). These publications take into account the spatial features of wireless networks, which is fundamentally different to many “classical” works on interference modeling and analysis (such as [12], [14]). The past years have also seen a branch of research that analyzes how interference *changes* over time and space [15]–[20]. Such *interference dynamics* can be described, for example, in terms of the autocorrelation of the received interference power (see [16], [21]). Correlation influences the system behavior, such as the performance of diversity, relaying, multiple-input multiple-output (MIMO), and MAC protocols (see [17], [18], [22], [23]).

Despite these advances in interference modeling, this new knowledge has not been exploited to actually improve the performance of wireless systems. The state of research is not as advanced as in channel modeling, where knowledge about the channel dynamics, such as coherence time and decorrelation distances, is indeed used in state-of-the-art technologies (e.g., space-time coding and MIMO). This gap from modeling to design is the motivation for our research: the investigation of concepts and solutions for interference prediction. At the core of our work is the fundamental issue: How well can we predict, in a probabilistic manner, the interference power at a given location in a given network into the future? An initial step in this direction is made in [24], where a simple prediction technique based on low-complexity learning of traffic patterns is proposed. The paper at hand presents a conceptually completely different predictor and discusses the problem more comprehensively.

B. Contributions and Overview

The key idea is to merge recent results on the autocorrelation of interference [21] with recursive filtering to predict the

Jorge F. Schmidt is with Lakeside Labs GmbH, Lakeside B04b, 9020 Klagenfurt am Wörthersee, Austria, E-Mail: schmidt@lakeside-labs.com.

Udo Schilcher is with the Institute of Networked and Embedded Systems, University of Klagenfurt, Lakeside B02a, 9020 Klagenfurt am Wörthersee, Austria and with Lakeside Labs GmbH, Lakeside B04b, 9020 Klagenfurt am Wörthersee, Austria, E-Mail: udo.schilcher@aau.at.

Mahin K. Atiq and Christian Bettstetter are with the Institute of Networked and Embedded Systems, University of Klagenfurt, Lakeside B02a, 9020 Klagenfurt am Wörthersee, Austria, E-mail: {mahin.atiq, christian.bettstetter}@aau.at.

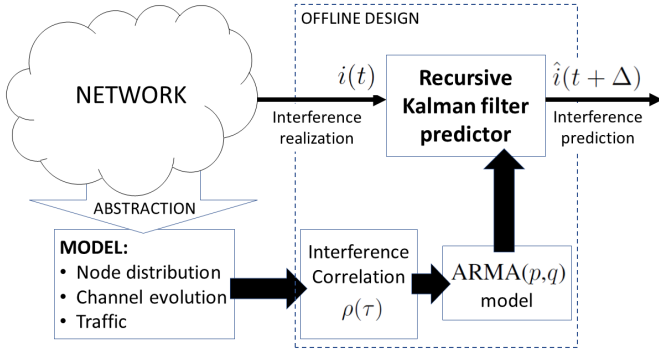


Fig. 1. Block diagram of the interference predictor.

level of interference into the future. Our contributions are as follows:

- A method is presented to map the autocorrelation function of interference into an autoregressive moving average (ARMA) model suited for performing forecasts from previous interference observations. This mapping is calculated for the case of Poisson distributed nodes, Rayleigh fading, and fixed message lengths.
- An offline and blind predictor is obtained by inserting the ARMA representation of the interference process into a Kalman filter. The time invariance of the model leads to a steady-state gain of the Kalman predictor to perform lightweight predictions at individual nodes.
- It is shown by simulations that the predictor outperforms basic prediction approaches as well as predictors that only account for the channel dynamics and disregard the impact of the network traffic.
- A sensitivity analysis demonstrates the robustness of the predictor against certain inaccuracies and model mismatches in its parameterization: it performs well with traffic and node distribution models that are more general than those used in its design.

A block diagram of the predictor design is given in Fig. 1.

The rest of the paper is organized as follows. Section II introduces the system model including the parameters defining the interference dynamics. Section III derives the interference predictor, starting with the stochastic geometry models of interference and progressing to the low-complexity recursive predictor implementation. Section IV evaluates the predictor performance in terms of accuracy; it includes a sensitivity analysis and specific technology examples. Finally, Section V provides conclusions and an outlook.

II. SYSTEM MODEL

A. System Setup

The system is described by the placement of nodes, their data traffic behavior, and a radio channel model. Time is discretized into slots $t \in \mathbb{N}_0$.

Nodes are distributed in a given area and move with a speed ν following a time-discrete Brownian motion model [25]. The

location x of a node at time $t + \tau$ is $x_{t+\tau} = x_t + \nu\omega_\tau$, with

$$\omega_\tau = \sum_{t=1}^{\tau} \omega_t \stackrel{d}{=} \sqrt{\tau}\omega_0, \quad (1)$$

where $\stackrel{d}{=}$ denotes equality in distribution and ω_t are i.i.d. two-dimensional Gaussian random variables of zero mean and covariance matrix

$$\Sigma = \begin{pmatrix} 0 & \sqrt{\frac{2}{\pi}} \\ \sqrt{\frac{2}{\pi}} & 0 \end{pmatrix}. \quad (2)$$

Each of the nodes is either transmitting or idle at a given time t . The interference power $i(t)$ at location ξ is caused by the set of transmitting nodes (interferers). Each idle node decides independently from other nodes whether to start a new transmission of a message in the next time slot. On average, a fraction μ of all nodes starts a new transmission. The message duration is $\ell \in \mathbb{N}$ slots. The wireless channel is described by a standard model that includes path loss and small-scale fading. A message transmitted at location x with power κ causes interference at ξ with power

$$i_\xi(t) = \kappa g(x, \xi) h_x^2(t) \quad (3)$$

with a distance-dependent path gain $g(x, \xi)$ and a random variable h describing signal fading due to multipath propagation caused by reflections, diffraction, and other effects as well as mobility of obstacles.

The parametrization of the predictor is done for the following special case of the system model: The nodes are randomly distributed according to a Poisson point process (PPP) Φ of intensity λ . Such node placement with random access is of widespread use in the literature to approximate wireless sensor networks. In recent years this model has also been intensively applied (with some considerations) to the analysis of cellular networks in general and to device-to-device communication technologies in particular (see [26]–[31]). The message duration ℓ is the same for all transmissions, which yields an expected traffic intensity of $\mu\ell$ interferers in each slot. The path gain is modeled by $g(x, \xi) = \|x - \xi\|^{-\alpha}$ with path loss exponent $\alpha > 2$ and assuming some normalization. Small-scale fading is modeled by Rayleigh fading with $\mathbb{E}[h^2(t)] = 1$. The reception power is then exponentially distributed. The widespread Jakes Doppler model [32] describes the continuous time evolution of the wireless channel. It assumes uniform scatterers directions which make it fit well a wide range of propagation environments. Its autocorrelation function is given by

$$\rho_J(\tau) = J_0(2\pi\tau\nu_{\max}), \quad (4)$$

where $J_0(\cdot)$ is the zeroth order Bessel function of the first kind and $\nu_{\max} = \nu$ the maximum expected mobile speed. We define η as the time lag for which the channel autocorrelation function first reaches zero. This system model is called base system in the following.

B. Interference

The overall interference at location ξ at time t is the sum of the reception powers at ξ from all transmitting nodes. In the case of Poisson networks, the consideration of a typical location ξ is equal to the consideration at the origin o of the plane \mathbb{R}^2 due to Slivnyak's theorem (see [33], [34]). With the given setup, the overall interference can thus be written as:

$$i(t) = \sum_{x \in \Phi} \kappa \|x\|^{-\alpha} h_x^2(t) \gamma_x(t), \quad (5)$$

where $\gamma(t)$ is a Bernoulli random variable indicating whether node x is sending ($\gamma_x(t) = 1$) at time t or not ($\gamma_x(t) = 0$), condensing the information from the parameters μ and ℓ . The interference process in (5) is stationary [34] and changes over time due to the time varying characteristics of the radio channel and the traffic. These sources of time varying behavior are captured by parameters η , μ , and ℓ .

III. INTERFERENCE PREDICTION

A. Interference Correlation

One of the main approaches for channel prediction is based on the exploitation of the autocorrelation characteristics of the channel [35]. We take a similar approach for interference prediction: our design starts from an analytical model for the autocorrelation function associated to the interference process. The autocorrelation of $i(t)$ for two time instants t_1 and t_2 can be given in terms of Pearson's correlation coefficient

$$\rho(i(t_1), i(t_2)) = \frac{\text{cov}[i(t_1), i(t_2)]}{\sigma_i^2}, \quad (6)$$

where $\text{cov}[i(t_1), i(t_2)] = \mathbb{E}[i(t_1)i(t_2)] - \mathbb{E}[i(t_1)]\mathbb{E}[i(t_2)]$ is the covariance of i , σ_i^2 its variance, and $\mathbb{E}[i]$ its expected value. The correlation lag is denoted by $\tau = t_2 - t_1$.

Expressions for this correlation are derived in [21] in a variety of system setups. The system model that parametrizes our predictor corresponds to Case (2, 2, 2) in [21], for which

$$\rho(i(t_1), i(t_2)) = \frac{\mathbb{E}[h^2(t_1)h^2(t_2)] \mathbb{E}[\gamma(t_1)\gamma(t_2)]}{\mu \ell \mathbb{E}[h^4(t)]} \cdot \frac{\int_{\mathbb{R}^2} g(x) \mathbb{E}[g(x + \nu\omega_\tau)] dx}{\int_{\mathbb{R}^2} g(x)^2 dx}, \quad (7)$$

where stationarity implies $\rho(i(t_1), i(t_2)) = \rho(i(t_2 - t_1))$, which we denote $\rho(\tau)$ in what follows. The channel contribution is $\mathbb{E}[h^2(t_1)h^2(t_2)] = J_0^2(2\pi\tau\nu_{\max}) + 1$. From this, and using [21, Th.2] we obtain the interference correlation function for the case where the channel is the sole source of correlation as $\rho(\tau) = J_0^2(2\pi\tau\nu_{\max})$. The traffic contribution is

$$\mathbb{E}[\gamma(t_1)\gamma(t_2)] = \max(0, \mu(\ell - \tau)) + \frac{\mu^2}{1 - \mu(\ell - 1)} \sum_{i=0}^{\min(\tau-1, \ell-1)} \sum_{j=1}^{\min(\tau-i, \ell)} \sum_{k=0}^{\lfloor \frac{g}{\tau} \rfloor} \binom{g-k\ell+k}{k} \beta^{g-k\ell} (1-\beta)^k,$$

with $g = \tau - i - j$, and $\beta = 1 - \mu/(1 - \mu(\ell - 1))$ being the probability of having a slot with all nodes being idle.

Table I shows three combinations of parameter values to be used in this paper. The first setup yields a highly correlated

interference, the second a moderate correlation, and the third a low correlation. These setups are used to illustrate some design steps and to assess the performance of the interference predictor.

TABLE I
EXAMPLE SETUPS

Setup	ν (m/slots)	μ	ℓ	η
1	0.0077	0.01	10	50
2	0.0191	0.01	10	20
3	0.0765	0.01	10	5

Fig. 2 illustrates the impact of different correlation sources for the overall interference. The upper plot shows the interference resulting from a time-varying channel (node mobility) and time-varying traffic. The lower plot shows the interference resulting from a time-varying channel only, with all nodes transmitting all the time. The visible differences between the traces in this example highlight the limitations of channel prediction in an interference-dominated system.

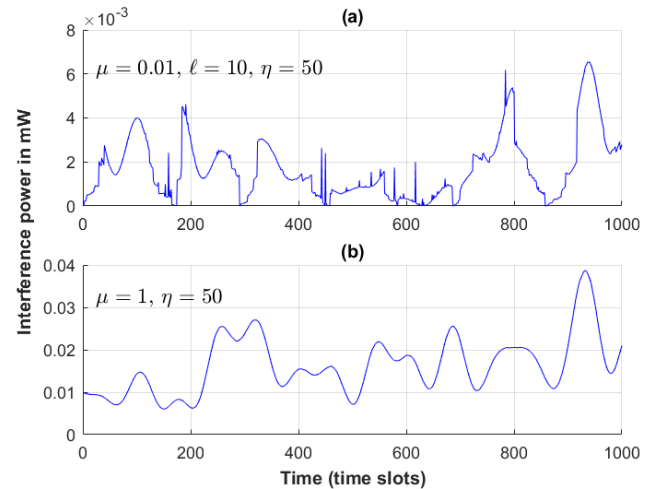


Fig. 2. Example interference traces depicting the impact of traffic on the interference dynamics. Part (a) shows a realization of Setup 1 from Table I. Part (b) shows a realization of Setup 1 that ignores the traffic contribution ($\mu = 1$) and only accounts for the channel dynamics.

We now explain the design of an interference predictor that harnesses the knowledge of the correlation expression (7) and is practically feasible in a sense that nodes can implement the predictor with limited computational resources and without additional signaling overhead.

B. ARMA Approximation of $\rho(\tau)$

ARMA models are extensively used in applications involving temporal stochastic processes. The Cramer-Wold theorem [36, Ch. 17] states that every stationary stochastic process has a moving average (MA) representation. When an autoregressive (AR) component is also used, the ability to accurately represent the process with a limited number of parameters greatly increases, making ARMA models particularly useful.

Typically, the ARMA representation of a process is identified from observing one of its realizations; the autocorrelation

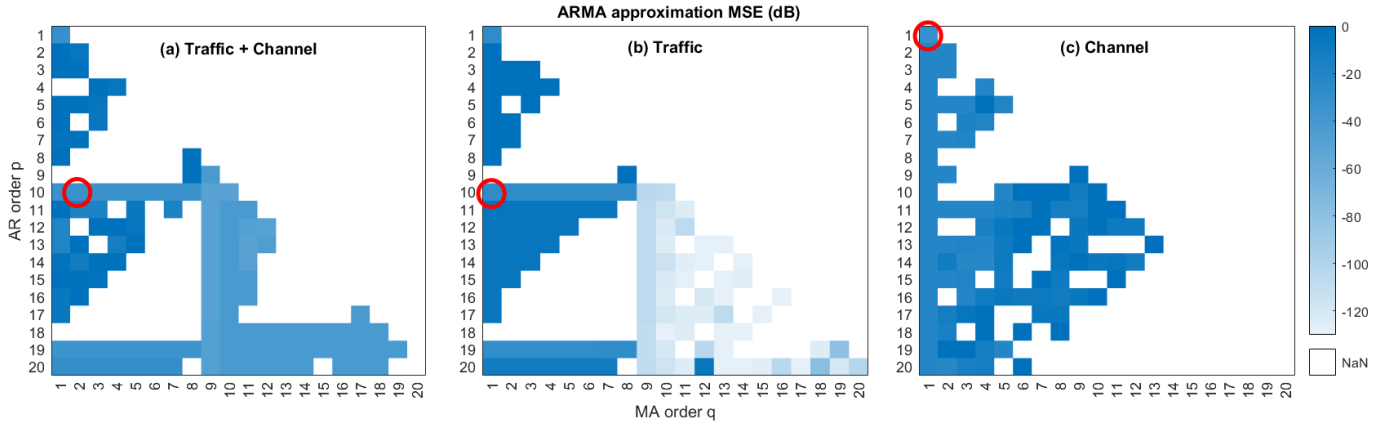


Fig. 3. Heatmaps showing the ARMA approximation MSE (dB) achieved by different (p, q) choices on three autocorrelation functions. Part (a) corresponds to for Setup 1 from Table I, part (b) for Setup 1 simplified to have time-invariant channel conditions, and part (c) for the simplification of Setup 1 to have time invariant traffic. The selected model orders, meeting an MSE target of -30 dB, are highlighted with red circles.

of the process is in general not known. Such identification approach entails the need of having several observations available from which to identify the model dimension and its coefficients values. These observations constitute a form of pilot signaling and can become impractically large in some cases, depending on the dynamics of the process to represent. Different to the typical case, we know $\rho(\tau)$ for a given system model in terms of the sources of correlation considered in (7). We are therefore interested in approximating it through an ARMA model with a limited number of parameters.

The ARMA(p, q) representation of $i(t)$ can be written as

$$\sum_{n=0}^p a_n i(t-n) = \sum_{n=0}^q b_n \epsilon(t-n), \quad q \leq p, \quad (8)$$

where the model orders p and q that achieve the equality are in principle not known. The coefficients a_n and b_n specify the AR and MA components of the model, respectively, and $\epsilon(t)$ is a zero-mean white noise process. The model is normalized by setting $a_0 = b_0 = 1$.

The coefficients in (8) can be inferred from $\rho(\tau)$. Specifically, multiplying (8) by $i(t-\tau)$ and taking expectation yields

$$\sum_{n=0}^p a_n \rho(\tau-n) = \sum_{n=0}^q b_n \delta(n-\tau), \quad (9)$$

with the Dirac delta function $\delta(\cdot)$. Specializing for $\tau = q + 1, \dots, q + p$, the AR coefficients a_1, \dots, a_p can be found as the solution to the resulting Yule-Walker equations [37] (see Appendix A for calculation details).

In order to determine the MA coefficients, an auxiliary sequence $\psi(t)$ defined to equal each side of (8) is introduced. Then:

$$\begin{aligned} \mathbb{E}[\psi(t)\psi(t-\tau)] &= \sum_{m=0}^p \sum_{n=0}^p a_m a_n \rho(\tau+n-m) \quad (10) \\ &= \sigma_\epsilon^2 \sum_{m=0}^q b_m b_{m+\tau}. \quad (11) \end{aligned}$$

Since all terms in the right hand side of (10) are known, by equating that expression to (11), the terms b_1, \dots, b_q and σ_ϵ^2 can be solved for (see Appendix A).

Note from (9) and (10) that only the first $p+q$ values of $\rho(\tau)$ are involved in the computation of the model coefficients. For a good representation, $p+q$ should be large enough to capture the main features of $\rho(\tau)$. If significant correlation exists for large τ values, a decimation of $\rho(\tau)$ can be performed to shorten the number of significant correlation lags prior to the parameter determination, to keep $p+q$ low. A scaling down in frequency of the resulting ARMA model in the same decimation factor is then performed to rescale the result.

C. ARMA Model Order Selection

The model orders p and q are unknowns used as design parameters. The described coefficient determination depends on these orders and is therefore not unique. Each (p, q) -combination results in a certain approximation error for $\rho(\tau)$, and several combinations result in very low approximation error. However, not all (p, q) -pairs are suitable.

The availability of $\rho(\tau)$ allows a least square approach to select the p and q . The feasible p and q combinations are those for which $\hat{\rho}_{p,q}(\tau) \rightarrow \rho(\tau)$ for $\tau \rightarrow \infty$. For this set, and a largest significant correlation lag of T , the mean square approximation error for pair (p, q) is

$$\text{MSE}(p, q) = \frac{1}{T} \sum_{\tau=1}^T (\rho(\tau) - \hat{\rho}_{p,q}(\tau))^2. \quad (12)$$

Pair (p, q) is then chosen as that lowest order- p model meeting a target approximation error. This selection criteria is illustrated in Fig. 3 for three different autocorrelation functions derived from Table I, considering a model order of up to $p = 20$, and $T = 100$. These examples show how the model order is affected by the different sources of correlation.

To obtain the approximation errors in Fig. 3, it is necessary to find the autocorrelation $\hat{\rho}_{p,q}(\tau)$ in (12) associated to a given (p, q) -combination, which we simply call $\hat{\rho}(\tau)$ in the

following. Using $\hat{\rho}(\tau)$ in (9) and noting that $\delta(n - \tau) = \mathbb{E}[i(t - \tau)\epsilon(t - n)] = 0$ for $\tau > n$, it follows that

$$\sum_n a_n \hat{\rho}(\tau - n) = 0 \quad \text{for } \tau > q. \quad (13)$$

Therefore, knowing the $q + 1$ nonzero values of $\delta(\cdot)$ and the p initial values of $\hat{\rho}(\cdot)$, (13) can be solved recursively for all values of $\hat{\rho}(\cdot)$ beyond p that are needed to compute (12).

To obtain the required nonzero δ -values, we follow [36, Ch. 17]. Multiplying (8) by $\epsilon(t - \tau)$ and taking expectation yields

$$\sum_{n=0}^{\tau} a_n \delta(\tau - n) = \sigma_\epsilon^2 b_\tau, \quad (14)$$

which can be rearranged as

$$\delta_\tau = \frac{1}{a_0} \left(b_\tau \sigma_\epsilon^2 - \sum_{n=0}^{\tau} a_n \delta(\tau - n) \right), \quad (15)$$

to recursively find $\delta(0), \delta(1), \dots, \delta(q)$. The p initial values of $\hat{\rho}(\cdot)$ are obtained by substituting $\delta(0), \delta(1), \dots, \delta(q)$ and $\hat{\rho}(\cdot)$ in (9). Finally, the initial values of $\hat{\rho}(\cdot)$ are used to compute the succeeding ones using (13).

D. Recursive Interference Predictor

An efficient interference predictor can be constructed from the derived ARMA(p, q) approximation of the interference process. Expressing the model coefficients as polynomials in the lag operator L and provided that the roots of the polynomial on a_n are outside the unit circle, the interference sequence results the filtered output of the noise sequence $\epsilon(t)$:

$$i(t) = \frac{b_0 + b_1 L + \dots + b_q L^q}{a_0 + a_1 L + \dots + a_p L^p} \epsilon(t). \quad (16)$$

This filter form suggest that it is possible to predict interference samples $\hat{i}(t + \Delta)$ by feeding the filter in (16) with a white noise sequence. However, such open loop prediction has poor accuracy given the sample autocorrelation dispersion between different realizations of the interference process. Nevertheless, a closed loop Kalman formulation of the filtering problem gives accurate predictions as will be shown in the next section.

For deriving the Kalman filter recursion, we first map our ARMA model into a state space form:

$$\mathbf{x}(t+1) = \mathbf{A}\mathbf{x}(t) + \mathbf{B}\epsilon(t) \quad (17)$$

$$i(t) = \mathbf{C}\mathbf{x}(t), \quad (18)$$

with state vector \mathbf{x} of size $p \times 1$, transition matrix

$$\mathbf{A} = \begin{bmatrix} a_1 & a_2 & \cdots & a_{p-1} & a_p \\ 1 & 0 & \cdots & 0 & 0 \\ 0 & 1 & \cdots & 0 & 0 \\ \vdots & \vdots & \ddots & \vdots & \vdots \\ 0 & 0 & \cdots & 1 & 0 \end{bmatrix}, \quad (19)$$

and $\mathbf{B} = [1 \ 0 \ \cdots \ 0]^T$ and $\mathbf{C} = [0 \ \cdots \ 0 \ b_0 \ \cdots \ b_q]$ of length p .

Assuming unitary process and measurement noise and following [38], the Kalman recursion for tracking $i(t)$ can be initialized with an all zeros state vector and a initial error

covariance $\mathbf{P} = \mathbf{B}\mathbf{B}^T$. At each iteration of the filter, the measurement update is

$$\mathbf{M} = \mathbf{P}\mathbf{C}^T (\mathbf{C}\mathbf{P}\mathbf{C}^T + 1)^{-1} \quad (20)$$

$$\mathbf{x}(t) = \mathbf{x}(t) + \mathbf{M}(i(t) - \mathbf{C}\mathbf{x}(t)) \quad (21)$$

$$\mathbf{P} = (\mathbf{I}_p - \mathbf{M}\mathbf{C})\mathbf{P}, \quad (22)$$

with the innovation gain \mathbf{M} and identity matrix \mathbf{I}_p of size p . The time update is

$$\mathbf{x}(t+1) = \mathbf{A}\mathbf{x}(t) + \mathbf{B}(i(t) - \mathbf{C}\mathbf{x}(t)) \quad (23)$$

$$\mathbf{P} = \mathbf{A}\mathbf{P}\mathbf{A}^T + \mathbf{B}\mathbf{B}^T. \quad (24)$$

Since the interference model is time invariant the error covariance \mathbf{P} converges to a constant [38] and (20) to (24) reduce to a steady-state Kalman filter of gain \mathbf{K}

$$\mathbf{x}(t+1) = \mathbf{A}\mathbf{x}(t) + \mathbf{K}(i(t) - \mathbf{C}\mathbf{x}(t)). \quad (25)$$

The interference prediction for a prediction horizon Δ can finally be found by extrapolating the state vector Δ time slots into the future on each iteration and using (18):

$$\tilde{\mathbf{x}} = \mathbf{A}^{\Delta-1} \mathbf{x}(t+1), \quad \hat{i}(t+\Delta) = \mathbf{C}\tilde{\mathbf{x}}. \quad (26)$$

The gain \mathbf{K} can be computed offline, which reduces the online effort of the predictor to the state update in (25) only, and the extrapolation of the filter through (26).

Reconsider the block diagram in Fig. 1 to summarize how the design steps are related. From a network model abstraction the interference autocorrelation function is obtained from (7). This correlation is used to parametrize an ARMA(p, q) model that is finally inserted into a steady-state Kalman filter to complete the offline design of the predictor. Predicted interference samples $\hat{i}(t + \Delta)$ are filtered samples of $i(t)$.

IV. EVALUATION OF INTERFERENCE PREDICTION

A. Evaluation in the Base System Model

We now investigate the performance of the interference predictor. As a first step, we apply the predictor to the base system that was used for its parameterization: PPP, Rayleigh fading, and fixed message lengths. The setups from Table I are used with a node density of $\lambda = 0.01$ over an area of 10,000 square units, a path loss exponent $\alpha = 3$, and all nodes using unitary transmit power $\kappa = 1$.

The prediction performance is evaluated in terms of the normalized mean square error:

$$\text{NMSE} = \frac{\sum_t (i(t+\Delta) - \hat{i}(t+\Delta))^2}{\sum_t i(t+\Delta)^2}, \quad (27)$$

which is a commonly used metric in channel prediction [35], as the normalization with the power of the input signal allows to average realizations with different powers. Error results are always averaged over 10,000 network realizations with 1,000 time slots interference sequences each.

Figure 4 plots the NMSE in Decibel (dB) over the prediction horizon in slots. Three predictors are compared: the interference predictor, a channel predictor, and a last value predictor. The channel predictor uses the same methodology but with $\rho(\tau)$ accounting for the channel as the sole source

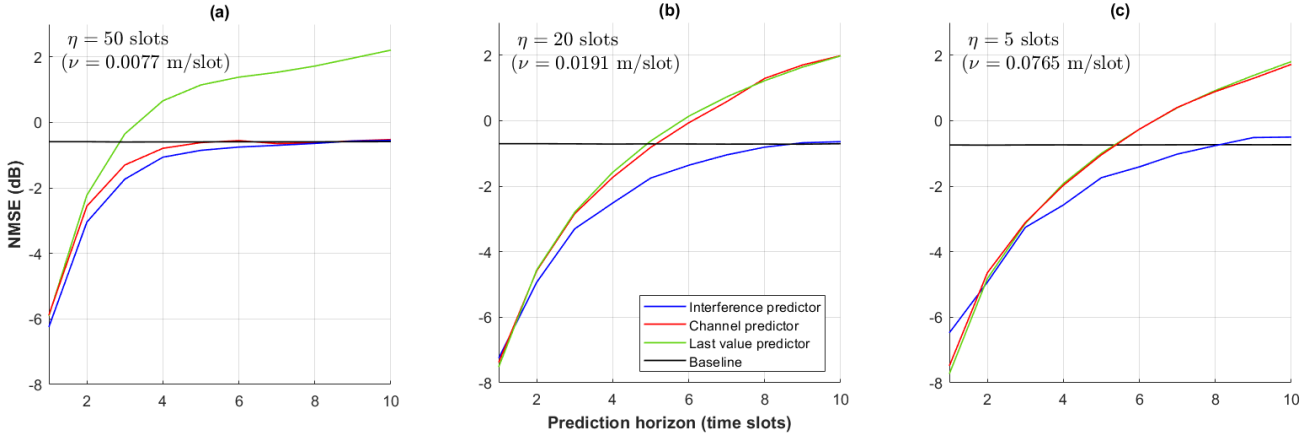


Fig. 4. Predictor evaluation for increasing node mobility. Comparison between the proposed interference predictor (blue), a channel predictor that ignores the traffic influence (red), and a predictor that outputs as prediction its current observation (green). The baseline of using the mean value of the interference as prediction is shown for reference.

of correlation (i.e., $\mu = 1$), which illustrates the impact of ignoring the traffic. The last value predictor simply takes its current interference observation as prediction. It is a performance reference for determining whether the low (but extra) complexity of the proposed predictor is justified. A “mean value predictor” serves as a baseline; it completely disregards interference dynamics and uses the mean value of the interference as prediction. As expected, the NMSE increases with an increasing prediction horizon for all three predictors in all setups. The interference predictor outperforms both the channel and last value predictors. Mobility increases from subplots (a) to (c) (i.e., setups 1 to 3 from Table I). The channel predictor gets close to the interference predictor for the low mobility scenario (a). For higher node speeds the channel predictor quickly degrades to the last value prediction reference. The interference predictor crosses the baseline in all cases for a prediction horizon of 8 slots, significantly larger than the 3 slots (Subfigure (a)) and 5 slots (Subfigures (b) and (c)) obtained for the last value predictor. This justifies its implementation cost.

Figure 5 deviates from Table I to explore the predictors behavior as the length of the messages changes. We consider Setup 1 with increasing message lengths. Longer messages result in higher interference correlation and thus lower prediction error. In all cases, the interference predictor outperforms the others, with predictors performance clustering together for longer messages. Note that for $\ell = 10$ the interference predictor attains horizons of 8 slots with an error below the baseline, whereas the last value and channel predictors cross above the baseline for an horizon of 5 slots.

Recalling that the model used for prediction is independent of the individual realizations of the interference process, Fig. 6 explores how the prediction error deviates from its average value in Figures 4 and 5 for different realizations of the network. While significant deviations exist for some realizations, most concentrate in the vicinity of the mean error.

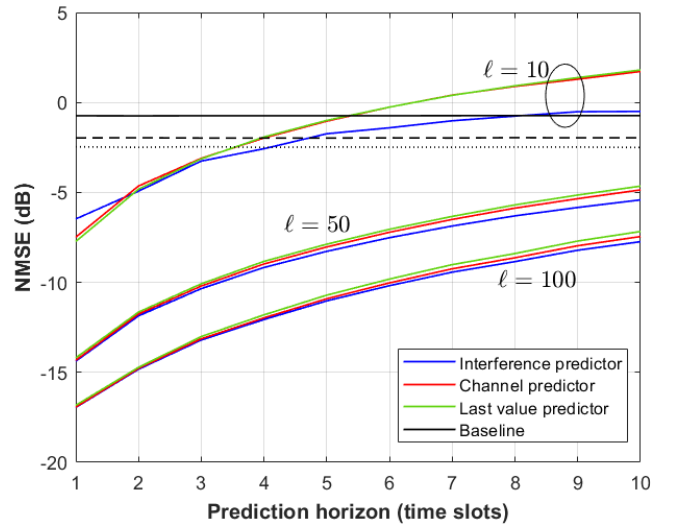


Fig. 5. Evaluation of the predictors for Setup 1 with different message lengths. The mean value predictor baseline is shown for reference with solid, dashed, and dotted trace for $\ell = 10$, 50, and 100, respectively.

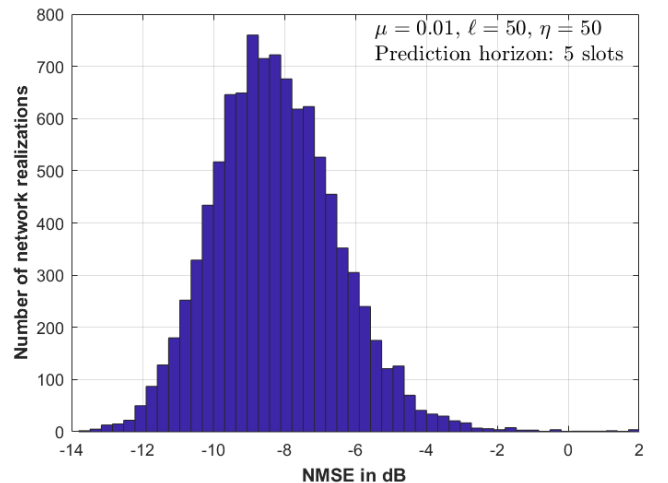


Fig. 6. NMSE distribution across network realizations. Results correspond to the case labeled $\ell = 50$ in Figure 5 with a prediction horizon of five time slots.

B. Sensitivity Analysis: Evaluation in Other System Models

We have seen that the interference predictor works well in the base system model that was used for its design. It is now of interest to evaluate as to whether it also works well in systems with other modeling assumptions. In other words, we are interested in how sensitive or robust the predictor is to variations or errors in the assumptions.

1) *System Model*: This is why we evaluate the predictor performance in (26) for the following models:

- The node locations are no longer a homogeneous PPP but show some inhomogeneity.
- The message lengths are no longer fixed to ℓ but are sampled from a Poisson distribution with parameter ℓ .

The modeling of the node locations is generalized by using an inhomogeneous random node distribution, in which nodes might be clustered in groups or concentrate around hotspots. Inhomogeneity is achieved by thinning the original PPP realizations, such that nodes with at least a certain number k of neighboring nodes within a distance r are kept [39]. Some examples are shown in Fig. 7 with fixed r and increasing k . Note that (7) does not contain λ , thus changes in the node density resulting from the thinning process do neither affect the interference correlation nor the predictor design.

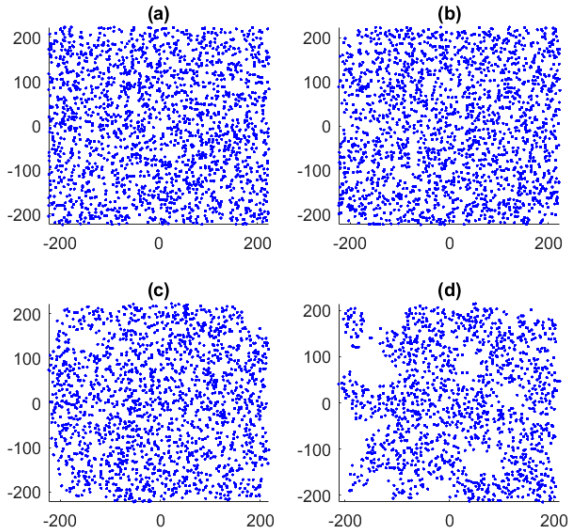


Fig. 7. Example network realizations where clustering between nodes is introduced. The original PPP (a) has an intensity $\lambda = 0.01$ over an area of 200,000 square units. Distance parameter r is set to 40 and neighbors cardinality k is set to 20 in (b), 30 in (c), and 40 in (d).

2) *Performance Results*: Figure 8 shows the NMSE of the proposed interference predictor for both setups when the interference samples at its input follow these alternative traffic and node placement models instead of the base system model. Subfigure (a) shows the impact of the design mismatch in terms of the inhomogeneous node distribution. The predictor exhibits a robust behavior for significantly high inhomogeneities. Deviations are marginal, and can only be appreciated in the figure for $k = 40$ (see Figure 7 (d)). Subfigure (b) reveals that the predictor is robust against the alternative traffic

model as long as the mean message length remains unchanged. The deviations are within the averaging noise.

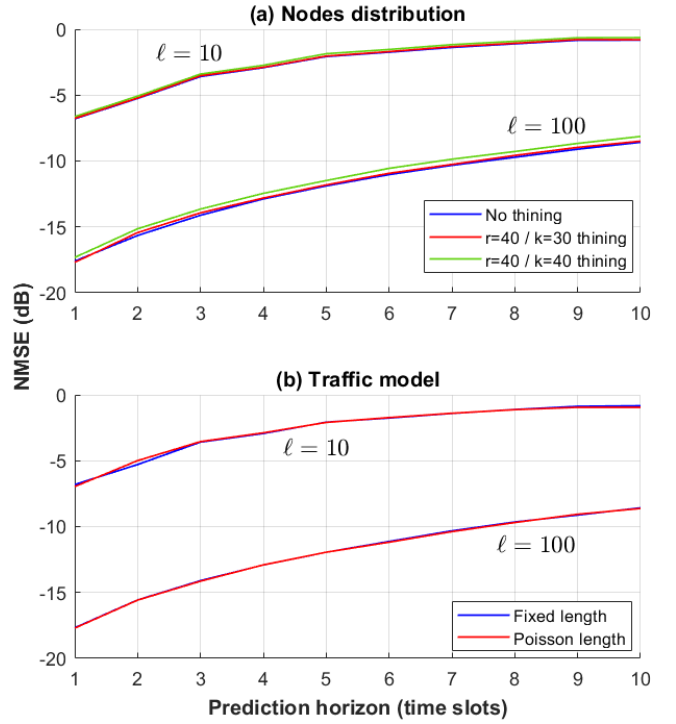


Fig. 8. Predictor sensitivity against (a) non-homogeneous nodes distribution and (b) Poisson distributed messages lengths. Results labeled $\ell = 10$ correspond to Setup 1 from Table I whereas those labeled $\ell = 100$ extend the message length of that setup.

C. Evaluation for Example Technologies

Finally, we investigate the performance for parameter values that are typical in two current wireless technologies: Long Term Evolution (LTE) used for cellular systems [40] and IEEE 802.15.4 used for wireless sensor networks (WSN) [41]. This evaluation will highlight the versatility of our predictor. We consider for this evaluation a message length of 20 slots.

1) *System Parameters*: Regarding LTE, we consider a downlink with carrier frequency f_c at the core 2 GHz band. A base station decides the nodes to schedule on a specific subcarrier (or block of contiguous subcarriers). Scheduling decisions can be made every millisecond, defining a time slot duration of one millisecond [40]. In order to effectively harness predictions at the base station, prediction horizons above five slots are required to compensate for the processing delays involved [42]. We consider pedestrian mobility with a maximum speed ν_{max} of 1,67 m/s (6 km/h), and vehicular speeds of 40 and 80 km/h. The maximum Doppler frequency can be calculated as

$$\Delta_f = \frac{2\nu_{max}}{c} f_c, \quad (28)$$

where $c = 3 \cdot 10^8$ is the speed of light. Table II summarizes the resulting parameter values.

Regarding the WSN, we consider a carrier frequency $f_c = 2.4$ GHz. The standard defines messages lengths of a minimum

TABLE II
LTE AND WSN SETUP

Scenario	ν (km/h)	μ	η	Δ_f^*
LTE 1	6	0.01	225	0.022
LTE 2	40	0.01	35	0.148
LTE 3	80	0.01	17	0.296
WSN	6	0.01	50	0.125

* Δ_f is normalized to the system time slot frequency.

of eight packets. With a packet duration of $577 \mu\text{s}$, a time slot duration of 4.6 ms results [41]. These values give a prediction horizon of 23 ms for predicting five slots ahead. We use the same pedestrian mobility as in LTE. The resulting parameters values are summarized in Table II.

2) *Performance Results*: Figure 9 shows the predictor performance for the two technologies. Shown is the ultimate predictor performance when we map the prediction horizons to the signal timing and expected channel dynamics from these technologies. We find that for both it is possible to predict beyond 5 slots ahead with an error below the mean interference baseline. The gains against the channel and last value predictor are in line with those in Figures 4 and 5.

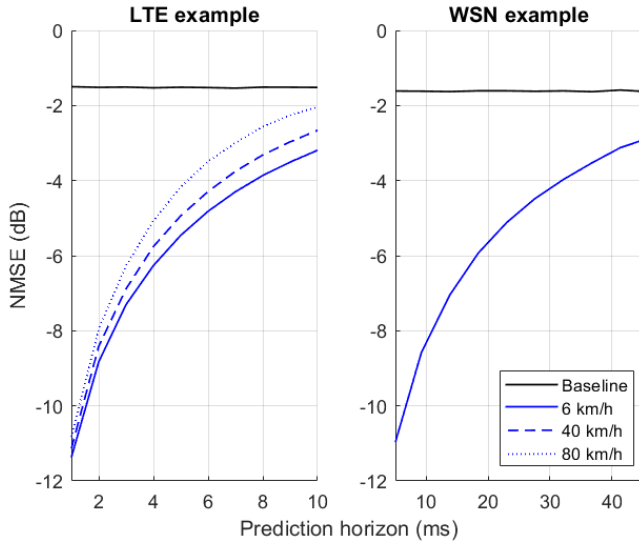


Fig. 9. Predictor performance for the different LTE and WSN scenarios from Table II.

V. CONCLUSIONS AND OUTLOOK

A novel methodology to exploit the stochastic characterization of interference dynamics for the design of a recursive interference predictor has been presented. The predictor can be implemented in the individual nodes due to its offline parametrization and low computational complexity. A performance analysis under matched and mismatched system conditions has demonstrated the prediction accuracy and robustness. Examples of prediction in LTE and sensor networks have confirmed the versatility of the design.

Ongoing work addresses additional theoretical and practical aspects of interference prediction. First, the presented predictor

will be implemented and tested in programmable radios. Second, the impact of interference prediction on the network dynamics will be studied: In contrast to channel prediction, the utilization of interference prediction by the nodes acts on the stochastic features of the interference process that is being predicted, and its effect needs to be accounted for.

APPENDIX A: MAPPING $\rho(\tau)$ TO AN ARMA(p, q) MODEL

Starting from (9) and following [36, Ch. 17], we let τ take values from 0 to $p + q$ to generate the following equation set

$$\begin{bmatrix} \rho(0) & \cdots & \rho(p) \\ \rho(1) & \cdots & \rho(0) \\ \vdots & & \vdots \\ \rho(q) & \cdots & \rho(p-q) \\ \vdots & \ddots & \vdots \\ \rho(q+p) & \cdots & \rho(q) \end{bmatrix} \begin{bmatrix} a_0 \\ a_1 \\ \vdots \\ a_p \end{bmatrix} = \begin{bmatrix} b_0 & b_0 & \cdots & b_0 \\ 0 & b_0 & \cdots & b_0 \\ \vdots & \vdots & \ddots & \vdots \\ 0 & 0 & \cdots & b_0 \\ \vdots & \vdots & & \vdots \\ 0 & 0 & \cdots & 0 \end{bmatrix} \begin{bmatrix} b_0 \\ b_1 \\ \vdots \\ b_q \end{bmatrix}. \quad (29)$$

Specializing for $\tau = q + 1, \dots, q + p$ we have

$$\begin{bmatrix} \rho(q) & \cdots & \rho(q-p+1) \\ \rho(q+1) & \cdots & \rho(q-p) \\ \vdots & \ddots & \vdots \\ \rho(q+p) & \cdots & \rho(q) \end{bmatrix} \begin{bmatrix} a_1 \\ a_2 \\ \vdots \\ a_p \end{bmatrix} = -a_0 \begin{bmatrix} \rho(q+1) \\ \rho(q+2) \\ \vdots \\ \rho(q+p) \end{bmatrix}, \quad (30)$$

which imposing $a_0 = 1$ can be recognized to be the Yule Walker equations to solve for for the AR coefficients a_1, \dots, a_p [37].

For determining the MA coefficients consider (10) and (11) from introducing sequence $\psi(t)$. Note that all terms are known from the solution of (30). Therefore, by running τ from 0 to q we can generate the required set of equations to solve for b_1, \dots, b_q and σ_ϵ^2 . These are

$$\begin{bmatrix} \psi(0) \\ \psi(1) \\ \vdots \\ \psi(q) \end{bmatrix} = \sigma_\epsilon^2 \begin{bmatrix} b_0 & b_1 & \cdots & b_{q-1} & b_q \\ b_1 & b_1 & \cdots & b_q & 0 \\ \vdots & \vdots & & \vdots & \vdots \\ b_q & 0 & \cdots & 0 & 0 \end{bmatrix} \begin{bmatrix} b_0 \\ b_1 \\ \vdots \\ b_q \end{bmatrix} \quad (31)$$

$$= \sigma_\epsilon^2 \begin{bmatrix} b_0 & b_1 & \cdots & b_{q-1} & b_q \\ 0 & b_0 & \cdots & b_{q-2} & b_{q-1} \\ \vdots & \vdots & & \vdots & \vdots \\ 0 & 0 & \cdots & 0 & b_0 \end{bmatrix} \begin{bmatrix} b_0 \\ b_1 \\ \vdots \\ b_q \end{bmatrix}, \quad (32)$$

which can be compactly written in matrix notation as

$$\boldsymbol{\psi} = \sigma_\epsilon^2 \mathcal{M}^\# \mathbf{b} = \sigma_\epsilon^2 \mathcal{M} \mathbf{b}, \quad (33)$$

where $\boldsymbol{\psi}$ and \mathbf{b} are the vector representation for sequence $\psi(t)$ and the MA coefficients, respectively in (31). $\mathcal{M}^\#$ and \mathcal{M} stand for the matrices in (31) and (32) respectively. The goal is to find the solution vector \mathbf{b} for the nonlinear system

$$\boldsymbol{\psi} - \sigma_\epsilon^2 \mathcal{M}^\# \mathbf{b} = 0. \quad (34)$$

The solution for (34) is found iteratively and in particular, we use the procedure from Tunnicliffe-Wilson [43] where the r th approximation to the solution is computed from the $(r - 1)$ th instance as

$$\mathbf{b}_r = \mathbf{b}_{r-1} + \{\sigma_\epsilon^2 (\mathcal{M}^\# + \mathcal{M})\}_{r-1}^{-1} (\boldsymbol{\psi} - \sigma_\epsilon^2 \mathcal{M}^\# \mathbf{b})_{r-1}. \quad (35)$$

As initialization we set $\sigma_\epsilon^2 = 1$ and $b_1 = b_2 = \dots = b_q = 0$ in (34). Upon convergence we normalize to have $b_0 = 1$.

ACKNOWLEDGMENTS

This work was supported with funding from the Austrian Science Fund (FWF) under grant P24480-N15 (Dynamics of interference in wireless networks); the Carinthian Economic Promotion Fund (KWF), the government of Styria, and the Styrian Business Promotion Agency (SFG) under grant FFG 864325 (UWB4Industry); and by the K-project DeSSnet (Dependable, secure and time-aware sensor networks), which is funded within the context of COMET – Competence Centers for Excellent Technologies by the Austrian Ministry for Transport, Innovation and Technology (BMVIT), the Federal Ministry for Digital and Economic Affairs (BMDW), and the federal states of Styria and Carinthia; the COMET program is conducted by the Austrian Research Promotion Agency (FFG).

REFERENCES

- [1] G. Zheng, I. Krikidis, C. Masouros, S. Timotheou, D.-A. Toumpakaris, and Z. Ding, “Rethinking the role of interference in wireless networks,” *IEEE Commun. Mag.*, vol. 52, no. 11, pp. 152–158, Nov. 2014.
- [2] A. B. Carleial, “A case where interference does not reduce capacity,” *IEEE Trans. Inf. Theory*, vol. 21, no. 5, pp. 572–584, Sep. 1975.
- [3] T. Han and K. Kobayashi, “A new achievable rate region for the interference channel,” *IEEE Trans. Inf. Theory*, vol. 27, no. 1, pp. 49–60, Jan 1981.
- [4] P. Minero, M. Franceschetti, and D. Tse, “Random access: An information-theoretic perspective,” *IEEE Trans. Inf. Theory*, vol. 58, no. 2, pp. 909–930, Feb. 2012.
- [5] V. R. Cadambe and S. A. Jafar, “Interference alignment and degrees of freedom of the k -user interference channel,” *IEEE Trans. Inf. Th.*, vol. 54, pp. 3425–3441, 2008.
- [6] M. Haenggi, “Mean interference in hard-core wireless networks,” *IEEE Commun. Lett.*, vol. 15, no. 8, pp. 792–794, Aug. 2011.
- [7] U. Schilcher, S. Toumpis, M. Haenggi, A. Crismani, G. Brandner, and C. Bettstetter, “Interference functionals in Poisson networks,” *IEEE Trans. Inform. Theory*, vol. 62, no. 1, pp. 370–383, Jan. 2016.
- [8] Y. Yang and A. Petropulu, “Co-channel interference modeling and analysis in a Poisson field of interferers in wireless communications,” *IEEE Trans. Signal Process.*, vol. 51, no. 1, pp. 64–76, 2003.
- [9] E. S. Sousa and J. A. Silvester, “Optimum transmission ranges in a direct-sequence spread spectrum multihop packet radio network,” *IEEE J. Sel. Areas Commun.*, vol. 8, no. 5, pp. 762–771, Jun. 1990.
- [10] R. Mathar and J. Mattfeldt, “On the distribution of cumulated interference power in Rayleigh fading channels,” *Wireless Netw.*, vol. 1, no. 1, pp. 31–36, 1995.
- [11] M. Hellebrandt and R. Mathar, “Cumulated interference power and bit-error-rates in mobile packet radio,” *Wireless Netw.*, vol. 3, no. 3, pp. 169–172, 1997.
- [12] K. A. Hamdi, “On the statistics of signal-to-interference plus noise ratio in wireless communications,” *IEEE Trans. Commun.*, vol. 57, no. 11, pp. 3199–3204, Nov 2009.
- [13] R. K. Ganti and M. Haenggi, “Interference and outage in clustered wireless ad hoc networks,” *IEEE Trans. Inf. Theory*, vol. 55, no. 9, pp. 4067–4086, Sep. 2009.
- [14] Y.-D. Yao and A. U. Sheikh, “Investigations into cochannel interference in microcellular mobile radio systems,” *IEEE Trans. Veh. Technol.*, vol. 41, no. 2, pp. 114–123, 1992.
- [15] R. Ganti and M. Haenggi, “Spatial and temporal correlation of the interference in ALOHA ad hoc networks,” *IEEE Commun. Lett.*, vol. 13, no. 9, pp. 631–633, Sep. 2009.
- [16] U. Schilcher, C. Bettstetter, and G. Brandner, “Temporal correlation of interference in wireless networks with Rayleigh fading,” *IEEE Trans. Mobile Comput.*, vol. 11, no. 12, pp. 2109–2120, Dec. 2012.
- [17] M. Haenggi and R. Smarandache, “Diversity polynomials for the analysis of temporal correlations in wireless networks,” *IEEE Trans. Wireless Commun.*, vol. 12, no. 11, pp. 5940–5951, Nov. 2013.
- [18] R. Tanbourgi, H. S. Dhillon, J. G. Andrews, and F. K. Jondral, “Effect of spatial interference correlation on the performance of maximum ratio combining,” *IEEE Trans. Wireless Commun.*, vol. 13, no. 6, pp. 3307–3316, Jun. 2014.
- [19] R. Tanbourgi, “Diversity combining under interference correlation in wireless networks,” Ph.D. dissertation, Karlsruhe Institute of Technology, Germany, Jun. 2015.
- [20] K. Koufos and C. P. Dettmann, “Temporal correlation of interference and outage in mobile networks over one-dimensional finite regions,” *IEEE Trans. Mobile Comput.*, vol. 17, no. 2, pp. 475–487, Feb. 2018.
- [21] U. Schilcher, J. F. Schmidt, M. K. Atiq, and C. Bettstetter, “Auto-correlation and coherence time of interference in Poisson networks,” *ArXiv e-prints*, Jun. 2018.
- [22] M. Haenggi, “Diversity loss due to interference correlation,” *IEEE Commun. Lett.*, vol. 16, no. 10, pp. 1600–1603, 2012.
- [23] R. Tanbourgi, H. S. Dhillon, J. G. Andrews, and F. K. Jondral, “Dual-branch MRC receivers under spatial interference correlation and Nakagami fading,” *IEEE Trans. Commun.*, vol. 62, no. 6, pp. 1830–1844, Jun. 2014.
- [24] M. K. Atiq, U. Schilcher, J. F. Schmidt, and C. Bettstetter, “Semi-blind interference prediction in wireless networks,” in *Proc. ACM Intern. Conf. on Modeling, Analysis and Simulation of Wireless and Mobile Systems (MSWiM)*, Miami Beach, FL, USA, Nov. 2017, pp. 19–23.
- [25] Z. Gong and M. Haenggi, “Interference and outage in mobile random networks: Expectation, distribution, and correlation,” *IEEE Trans. Mobile Comput.*, vol. 13, no. 2, pp. 337–349, Feb. 2014.
- [26] X. Lin, J. Andrews, and A. Ghosh, “Spectrum sharing for device-to-device communication in cellular networks,” *IEEE Trans. Wireless Commun.*, vol. 13, no. 12, pp. 6727–6740, Dec 2014.
- [27] H. ElSawy, E. Hossain, and M.-S. Alouini, “Analytical modeling of mode selection and power control for underlay D2D communication in cellular networks,” *IEEE Trans. Commun.*, vol. 62, no. 11, pp. 4147–4161, Nov 2014.
- [28] N. Lee, X. Lin, J. Andrews, and R. Heath, “Power control for D2D underlaid cellular networks: Modeling, algorithms, and analysis,” *IEEE J. Sel. Areas Commun.*, vol. 33, no. 1, pp. 1–13, Jan 2015.
- [29] M. Erturk, S. Mukherjee, H. Ishii, and H. Arslan, “Distributions of transmit power and SINR in device-to-device networks,” *IEEE Commun. Lett.*, vol. 17, no. 2, pp. 273–276, Feb 2013.
- [30] Q. Ye, M. Al-Shalash, C. Caramanis, and J. Andrews, “Resource optimization in device-to-device cellular systems using time-frequency hopping,” *IEEE Trans. Wireless Commun.*, vol. 13, no. 10, pp. 5467–5480, Oct 2014.
- [31] J. F. Schmidt, M. K. Atiq, U. Schilcher, and C. Bettstetter, “Underlay device-to-device communications in LTE-A: Uplink or downlink?” in *Proc. IEEE Int. Symp. Personal, Indoor, and Mobile Radio Commun. (PIMRC)*, Hong Kong, China, Sep. 2015, pp. 1542–1546.
- [32] W. Jakes, *Microwave Mobile Communications*. New York: Wiley, 1974.
- [33] D. Stoyan, W. S. Kendall, and J. Mecke, *Stochastic Geometry and its Applications*, 2nd ed. Wiley, 1995.
- [34] M. Haenggi and R. Ganti, *Interference in Large Wireless Networks*. now publishing, 2009.
- [35] A. Duel-Hallen, “Fading channel prediction for mobile radio adaptive transmission systems,” *Proceedings of the IEEE*, vol. 95, no. 12, pp. 2299–2313, Dec. 2007.
- [36] D. S. G. Pollock, *Time Series Analysis Signal Processing and Dynamics*. Academic Press Ltd, London, 1998.
- [37] P. A. Regalia, *Adaptive IIR Filtering in Signal Processing and Control*. Marcel Dekker, Inc., 1995.
- [38] C. Chui and G. Chen, *Kalman Filtering - with Real-Time Applications*. Springer-Verlag 2nd Ed, 1991.
- [39] C. Bettstetter, M. Gyarmati, and U. Schilcher, “An inhomogeneous node distribution and its stochastic properties,” in *Proc. ACM/IEEE Intern. Symp. on Modeling, Analysis, and Simulation of Wireless and Mobile Systems (MSWiM)*, Chania, Greece, Oct. 2007, pp. 400–404.
- [40] 3GPP TS 36.213, “Evolved universal terrestrial radio access: Physical layer procedures (Release 14),” Apr 2017.
- [41] IEEE Std 802.15.4, “Wireless medium access control and physical layer specifications for low rate wireless personal area networks,” Sept 2006.
- [42] J. F. Schmidt, J. E. Cousseau, R. Wichman, and S. Werner, “Bit loading using imperfect CSIT for prediction-based resource allocation in mobile OFDMA,” *IEEE Trans. Veh. Technol.*, vol. 60, no. 8, pp. 4082–4088, 2011.
- [43] G. Wilson, “Factorization of the covariance generating function of a pure moving average process,” *SIAM J. Numer. Anal.*, vol. 6, no. 1, pp. 1–7, 1969.